APPLIED SCIENCES AND ENGINEERING

Versatile adhesive skin enhances robotic interactions with the environment

Changhong Linghu[1]†, Yangchengyi Liu[1,2]†, Xudong Yang[1]†, Zhou Chen[3]†, Jin Feng[4], Yiyuan Zhang[5], Yan Li[1], Zhao Zhao[6], Young-Jae Seo[1], Junwei Li[1], Haoyu Jiang[1], Jiangtao Su[7], Yin Fang[8], Yuhang Li[9], Xiufeng Wang[2]*, Yifan Wang[1]*, Huajian Gao[10]*, K. Jimmy Hsia[1,8]*

Electronic skins endow robots with sensory functions but often lack the multifunctionality of natural skin, such as switchable adhesion. Current smart adhesives based on elastomers have limited adhesion tunability, which hinders their effective use for both carrying heavy loads and performing dexterous manipulations. Here, we report a versatile, one-size-fits-all robotic adhesive skin using shape memory polymers with tunable rubber-to-glass phase transitions. The adhesion strength of our adhesive skin can be changed from minimal (~1 kilopascal) for sensing and handling ultralightweight objects to ultrastrong (>1 megapascal) for picking up and lifting heavy objects. Our versatile adhesive skin is expected to greatly enhance the ability of intelligent robots to interact with their environment.

INTRODUCTION

The skin is the most crucial interface between the environment and both animals and robots. On the inside, natural skin contains mechanoreceptors that are critical for sensory perception such as light and touch or temperature and pressure. On the outer surface, it has appendages such as hair, nails, feathers, and scales that are essential for movement, lubrication, and protection (*1*, *2*). Adhesive skin appendages (*3*–*5*), for example, allow some animals like geckos, octopus, and suckerfish to adhere (*3*, *6*), parasitize (*7*, *8*), capture (*9*–*11*), and climb (*12*–*14*) on various surfaces. Such adhesive skin appendages that adhere strongly and yet can detach easily have inspired the creation of smart adhesives (*3*) that outperform friction-based designs (*15*–*17*). These adhesives have been applied in heterogeneous assembly (*18*–*24*), soft robots (*3*, *25*, *26*), and as soft grippers (*27*–*31*) to reliably grip and release large, heavy, or fragile objects. Similarly, tactile mechanoreceptors in skin tissues have inspired the development of electronic skins (E-skins)—flexible, stretchable electronic materials with sensing capabilities (*32*–*40*)—that have enabled robots to respond to strain, pressure, temperature, and other environmental stimuli (*41*–*45*).

The functional capabilities of current E-skins for robotics, however, are incomplete because they mimic mainly the sensory functions of natural skin yet are often missing the specialized functions such as adhesion. This is because current smart bioinspired adhesives, mostly made of soft elastomers (*46*), are often focused on a single function. The same adhesive cannot be effectively used both for carrying heavy loads and for dexterous manipulation of objects because the minimum and maximum adhesion strengths of these elastomers are proportional to each other (*47*, *48*), as illustrated in Fig. 1A (also see section S3). An adhesive with a maximum adhesion strength high enough to lift heavy loads usually has a high minimum adhesion strength, making a robot difficult to achieve human-like actions like grasping, carrying, and detaching small lightweight objects like cloth, paper, or microchips (*49*, *50*). In sensing applications (*51*–*53*), excessive adhesion can interfere with signal detection. Adhesive E-skins that mimic more closely the capabilities of real skin would greatly improve their values in various robotic applications, including prosthetics.

Here, we report a one-size-fits-all adhesive skin (Fig. 1B; see more details in fig. S1 and section S1) for robotics, which incorporates both sensory and adhesive functions for various manipulation scenarios. This is achieved by using shape memory polymers (SMPs) (*54*, *55*) with tunable rubber-to-glass (R2G) phase transition that enables the adhesive to adhere and detach on-demand. The surface layer of our adhesive skin is made of structured SMP fibrils resembling the natural adhesive skin appendages of tree frogs (*56*, *57*), providing a larger area filling ratio and consistent shear adhesion strength across various loading directions compared to other geometries. The phase transition of the SMP is regulated by a flexible heater layer and a flexible pressure sensor is used to accomplish the sensing function of the adhesive skin. Systematic studies and simulations show that the adhesion strength of our adhesive skin is tunable from ~1 kPa to ~1 MPa, allowing a robotic hand to detect surface morphologies and perform a wide range of tasks, from picking up a light (25 g) towel to grasping various fragile, large, curved (10 to 40 cm radii), and heavy (up to 1.2 kg) objects. Our robotic adhesive E-skin, with its integrated sensory and adhesive functions, offers huge potential across multiple industries, including manufacturing, construction, logistics, measurement, maintenance, and health care, by enhancing productivity, safety, and precision.

RESULTS

Design and operating principles

Robotic environments are highly complex, demanding adhesive skins with widely tunable adhesion capabilities. Conventional adhesive

[1]School of Mechanical and Aerospace Engineering, Nanyang Technological University, 50 Nanyang Avenue, Singapore 639798, Singapore. [2]School of Materials Science and Engineering, Xiangtan University, Xiangtan, Hunan 411105, China. [3]College of Mechanical and Electrical Engineering, China Jiliang University, Hangzhou 310018, China. [4]Department of Mechanical Engineering, Massachusetts Institute of Technology, 77 Massachusetts Avenue, Cambridge, MA 02139, USA. [5]Department of Mechanical Engineering, National University of Singapore, Singapore 117575, Singapore. [6]China Special Equipment Inspection and Research Institute, Beijing 100029, China. [7]School of Materials Science and Engineering, Nanyang Technological University, Singapore 639798, Singapore. [8]School of Chemistry, Chemical Engineering and Biotechnology, Nanyang Technological University, 50 Nanyang Avenue, Singapore 639798, Singapore. [9]Institute of Solid Mechanics, Beihang University, Beijing 100191, China. [10]Mechano-X Institute, Applied Mechanics Laboratory, Department of Engineering Mechanics, Tsinghua University, Beijing 100084, China.
*Corresponding author. Email: onexf@xtu.edu.cn (X.W.); yifan.wang@ntu.edu.sg (Y.W.); gao.huajian@tsinghua.edu.cn (H.G.); kjhsia@ntu.edu.sg (K.J.H.)
†These authors contributed equally to this work.

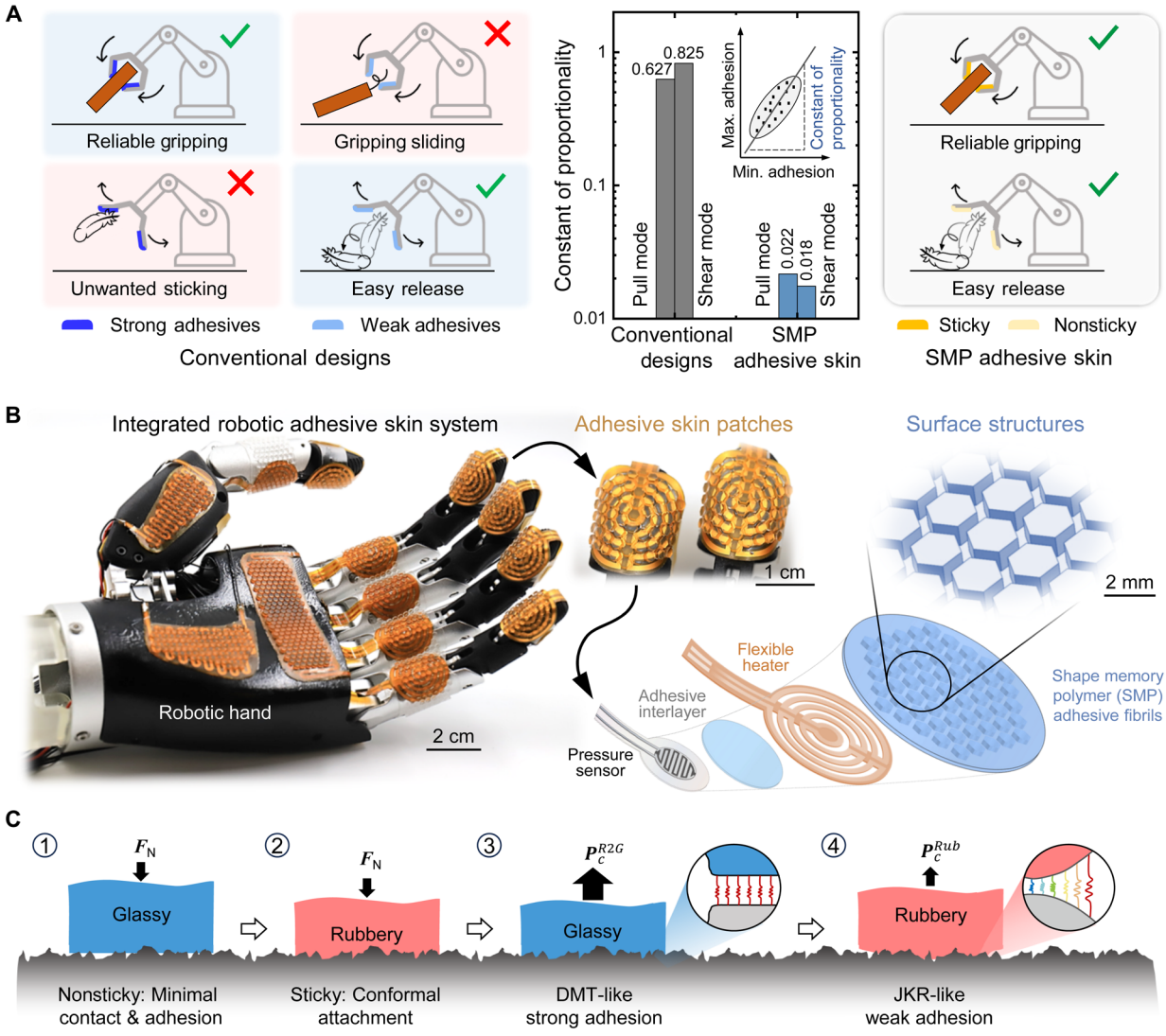

Fig. 1. Design and operation of SMP robotic adhesive skins. (**A**) Schematic comparison between the proposed SMP adhesive skin and conventional adhesive designs. In conventional adhesives designs (left), the maximum adhesion strength is proportional to the minimum strength, characterized by large constants of proportionality in both pull and shear modes (middle). This limitation means that strong adhesives and easy detachment cannot be achieved with the same adhesive. In contrast, the proposed SMP adhesive skin features maximum and minimum adhesion strengths that are independent of each other, with very small constants of proportionality (middle). This enables a wide tunability in adhesion, allowing the adhesive skin to function effectively in scenarios where adhesion is either required or to be avoided, thereby greatly enhancing robotic interactions (right). (**B**) SMP adhesive skins integrated onto a robotic hand (left) to enhance its capabilities to interact with the environment. The robotic adhesive skin patches (right) are featured by arrays of hexagonal SMP adhesive fibrils on the surface and then embedded flexible heaters and pressure sensors connected by SMP adhesive interlayers. (**C**) Principle of on-demand attachment and detachment of a single SMP adhesive fibril on the adhesive skin. ① Minimal adhesion when contacting in the glassy phase. ② On-demand attachment when contact is established in the rubbery phase. ③ Strong DMT-like R2G adhesion after cooling into the glassy phase. ④ Switch-off of adhesion by heating up back into the rubbery phase where the SMP fibrils are detached in a JKR-like state.

designs are limited because their maximum and minimum adhesion strengths are proportional to each other, with constants of proportionality as high as 0.627 and 0.825 in pull and shear modes, respectively (Fig. 1A). In contrast, our SMP adhesive skin demonstrates extraordinary adhesion capabilities with maximum and minimum adhesion strengths nearly independent of each other, reducing constants of proportionality by 29- and 45-fold in pull and shear modes, respectively. This remarkable tunability enables robots to have unprecedented interaction capabilities, allowing them to perform effectively whether adhesion is desirable or to be avoided.

The on-demand attachment and detachment of our adhesive skin relies on the tunable R2G phase transition of E44 Epoxy SMPs (E44-SMP). Although the highly tunable modulus, shape-locking, and shape memory effects of E44-SMP make it a promising adhesive, the material in our previous studies is not suitable for many robotic applications due to its high transition temperature (~90°C) (*48*, *58*) that may damage objects like fabrics and plasticware. To make the material more compatible with a wider range of objects, we adjusted the monomer-to-curing agent ratio of E44-SMP to 81:48 to lower the glass transition temperature to 36°C (fig. S2; see details in section S2).

In the glassy phase (temperature $T < 30$°C), the E44-SMP is stiff (storage modulus $E' > 1$ GPa) and does not attach to the adherend (Fig. 1C). When heated above 51°C to the soft rubbery phase, the SMP softens ($E' < 1$ MPa) and deforms to form conformal contact with the adherend under a preload. Such deformation can be locked when the SMP transitions back to the glassy phase. This leads to a Derjaguin-Muller-Toporov (DMT)-like adhesion regime (*48*, *58*), where the interfacial stress reaches close to the theoretical adhesion strength and achieves a strong R2G adhesion. Reheating the SMP back to the rubbery phase, the shape memory property leads to the return to the undeformed geometry, breaking the conformal contact, resulting in a Johnson-Kendall-Roberts (JKR)-like adhesion regime, where the interfacial stress is concentrated at the edge of the contact interface. Crack propagation and weak rubbery adhesion at this point facilitate detachment.

SMPs have recently gained significant attention in smart adhesives (*59*–*64*) due to their ultrastrong R2G adhesion, where contact occurs in the rubbery phase and detachment takes place in the glassy phase. This adhesion can also be switched on-demand to weaker rubbery adhesion, where both contact and detachment occur in the rubbery phase. Recently, Linghu *et al.* (*58*) uncovered that the enhancement of SMP R2G adhesion is dominated by the shape-locking effect. In addition, they (*48*) have shown that on-demand attachment is achieved through the softness of the rubbery SMP, whereas the stiffness of the glassy SMP enables a nonstick behavior with minimal contact area and low glassy adhesion, where both contact and detachment take place in the glassy phase.

Building on these theoretical insights, our adhesive skin leverages the tunable mechanical properties of E44-SMP, endowing it with a wide range of adhesion strengths. This versatility enables the robot to interact with the environment in multiple ways. The robotic adhesive skin can be made more adhesive when gripping fragile, large, or heavy objects or less adhesive when detecting surface texture or manipulating light objects, as shown later.

Characterization and optimization of SMP adhesive fibrils

As mentioned above, the key to enhancing robotic interactions lies in the tunability of adhesive skins. We fabricated SMP adhesive fibrils in the form of hexagonal pillars (edge length $a = 1$ mm with various aspect ratios) (fig. S4 and section S4) and experimentally characterized their glassy adhesion, rubbery adhesion, and R2G adhesion in pull and shear modes through systematic pull-off and shear tests (fig. S5 and section S5). Discrete fibrillar structures of this size can provide strong load capabilities for gripping and larger switchability for release, as previously demonstrated (*65*).

Figure 2A shows the influence of preload on the adhesion strength of SMP adhesive fibrils in pull and shear modes. In both modes, the R2G and rubbery adhesion strengths saturate at a small preload of about 38.5 kPa due to the softness of the SMP in the rubbery phase during contact. The R2G adhesion is measured to be around 2.0 MPa in pull mode and 5.1 MPa in shear mode, whereas the rubbery phase adhesion strength is 164.4 kPa in pull mode and 206.9 kPa in shear mode. The ratio between the maximum adhesion (i.e., the R2G adhesion) and the preload of the SMP fibrils is 90 at a preload of 19.2 kPa and 50 at 38.5 kPa, outperforming existing dry adhesives (ratio of around 1) and the state-of-the-art biomimetic designs using soft elastomers (ratio of about 6) (*66*). This wide adhesion range and large adhesion-to-preload ratio enable a robotic hand to reliably grip various objects, from fragile items such as eggs and shells to heavy objects such as steel balls. In contrast, the glassy adhesion reaches a maximum of 5.7 kPa in the pull mode and 20.5 kPa in the shear mode, even at high preload levels. Unlike R2G and rubbery adhesion, in the glassy phase, the adhesive force in shear mode increases linearly with preload further due to friction. The measured coefficient of friction is around 0.3803. If friction were used to grip an object, then insufficient preload would result in sliding and gripping failure, whereas high preloads required for reliable gripping could deform or damage the object. In scenarios where adhesion is undesirable, however, minimal adhesion force would be desirable.

As reported in (*67*), the fibril aspect ratio hugely influences the adhesion performance. In this study, adhesion tests on fibrils with various aspect ratios (fig. S6, A and B) showed that, in pull mode (fig. S6A), R2G adhesion is unaffected by the aspect ratio, whereas rubbery and glassy adhesion strengths decrease slightly with increasing aspect ratio. In shear mode (fig. S6B), when the aspect ratio is less than 1, deformation is block-shearing dominant (*67*) and adhesion strength shows limited dependence on the aspect ratio. However, when the aspect ratio exceeds 1, adhesion strength decreases rapidly due to beam bending deformation (*67*). Together, our results show that fibrils with smaller aspect ratios lead to stronger R2G adhesion but conform less well to different surface textures. In the current work, we used fibrils with an aspect ratio of 1 to ensure that R2G adhesion is maintained in both pull and shear modes.

In addition to glass substrates, we also characterized the R2G, rubbery, and glassy adhesion of SMP adhesives on steel, acrylic, and polypropylene (PP). SMP is known to adapt to different surfaces due to its shape-locking effect (*48*). On all surfaces, R2G adhesion exceeded 1 MPa (Fig. 2B). The rubbery adhesion is about 10 times lower than the R2G adhesion. The glassy adhesion is about 10 times lower than the rubbery adhesion. Because of the shape locking of the conformal contact during R2G adhesion (*48*, *58*), introducing surface roughness on the tips of the SMP fibrils (section S4) further reduces the rubbery and glassy adhesion without affecting R2G adhesion (fig. S6, C and D). As surface roughness [root mean square (RMS)] increases from 0.455 to 46.96 μm, rubbery adhesion drops from 164.4 to 4.3 kPa in pull mode and from 206.9 to 41.7 kPa in shear mode. Meanwhile, glassy adhesion decreases from 5.7 to 0.65 kPa in pull mode and from 20.5 to 2.86 kPa in shear mode. Such reductions allow adhesion strengths to be switched for on-demand gripping and release and for applications desiring low adhesion. The microroughness structures can fully recover and be used repeatedly due to the excellent shape memory performance of the E44-SMP, as shown in our previous works (*28*, *48*, *65*).

In conventional adhesives made of soft elastomers, adhesion forms upon contact. However, because the minimum adhesion (or detachment) strength for these materials increases with the maximum adhesion strength with large constants of proportionality (Fig. 2, C and D; see details in fig. S3 and section S3), they cannot be effectively used for both strong adhesion and nonadhesive applications. In contrast, the maximum and minimum adhesion strengths of SMP adhesives are nearly independent, as indicated by the small constants of proportionality already summarized in Fig. 1A. With the SMP adhesive, the ultrastrong R2G adhesion attained from the shape-locking effect would drop by one to two orders of magnitude when the adhesive is transformed to the rubbery phase (red stars in Fig. 2, C and D). Furthermore, in the glassy phase, the adhesion strength between the SMP adhesive and the substrate drops by an additional one to two orders of magnitude (blue stars in Fig. 2, C and D). The

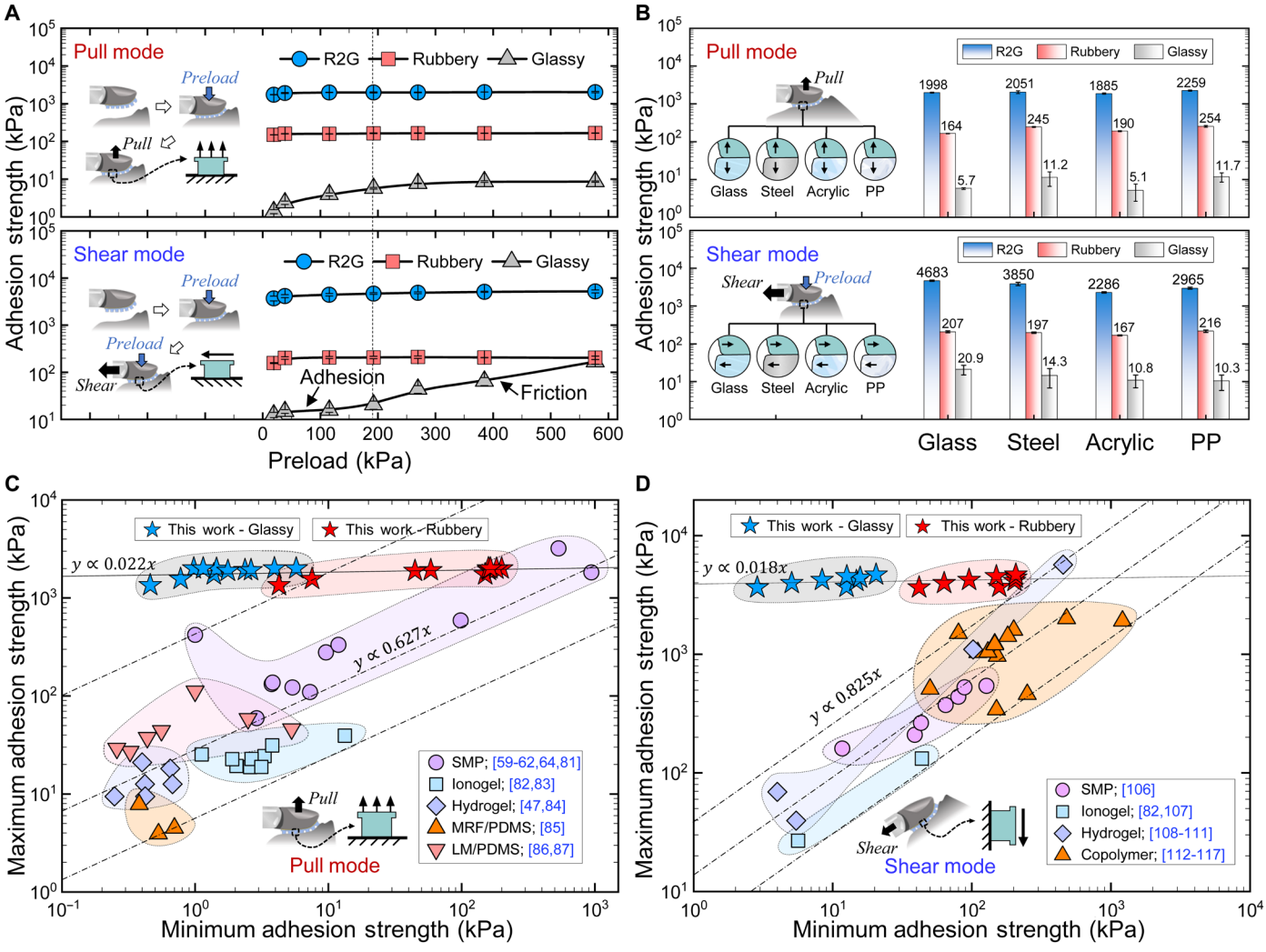

Fig. 2. Adhesion performance of SMP fibrils. (**A**) Influence of preload on adhesion strength under pull (top) and shear (bottom) modes (measured on smooth glass, aspect ratio = 1). Vertical dashed lines indicate the preload where glassy adhesion saturates. R2G and rubbery adhesions saturate under a small preload (<38.5 kPa), whereas glassy adhesion remains unsaturated even at a large preload of 206.9 kPa. In pull mode, saturated glassy adhesion remains below 10 kPa. In shear mode, glassy adhesion increases with preload due to friction, approaching rubbery adhesion at an extremely high preload of 577.4 kPa. (**B**) Adhesion strength on various substrates under pull (top) and shear (bottom) modes (aspect ratio = 1 and preload = 192 kPa). Adhesion characteristics, including high R2G adhesion, low rubbery adhesion, and minimal glassy adhesion, are consistent across substrates. (**C** and **D**) Comparison of minimum and maximum adhesion strengths of SMP fibrils under (C) pull and (D) shear modes, against other adhesives made from various materials. In conventional smart adhesives, the minimum adhesion strength increases as the maximum adhesion strength increases with a large constant of proportionality (also see Fig. 1A), limiting the range of adhesion tunability. (Details of literature data for elastomers are available in sections S1 and S2.) In contrast, in the proposed smart adhesive for robotic skin using phase transition in SMP, the maximum adhesion strength is achieved through the R2G phase transition, independent of the minimum adhesion, featuring small constants of proportionality (also see Fig. 1A). The maximum adhesion exceeds 1 MPa, whereas the minimum adhesion strength is tunable to as low as 4.26 kPa (rubbery phase) and 0.46 kPa (glassy phase) in pull mode and 41.7 kPa (rubbery phase) and 2.87 kPa (glassy phase) in shear mode.

wide and tunable adhesion range (0.65 kPa to 2 MPa in pull mode and 2.86 kPa to 5.1 MPa in shear mode) of the SMP adhesive outperforms existing smart adhesives (see details in fig. S3, C and D; tables S1 and S2; and section S3), enhancing robots' adaptability and functionality in interacting with complex environments, be adhesion desirable or not.

SMP fibril attachment and detachment on-demand

The wide range of adhesion strength in different phases is attributed to the tunable modulus of the adhesive, which spans three orders of magnitude, allowing them to attach on and detach from surfaces on-demand (Fig. 3A). In the glassy phase, the SMP is stiff (E' ~2 GPa) and nonsticky. Contacts in this state exhibit minimal adhesion, useful for applications that require low or no adhesion. When heated to the rubbery phase, the SMP softens (E' ~1 MPa) and forms sticky contact with the adherend. Such sticky contact achieves intermediate adhesion strength according to the Dahlquist criterion (*48*). To further understand how the SMP switches from nonsticky to sticky conditions, we examined the adhesive interactions between an SMP fibril and common substrates under near zero loading as a function of the stickiness parameter, χ (see details in Materials and Methods, fig. S7, and section S6) (*68*). For $\chi > 1$, the adhesive is

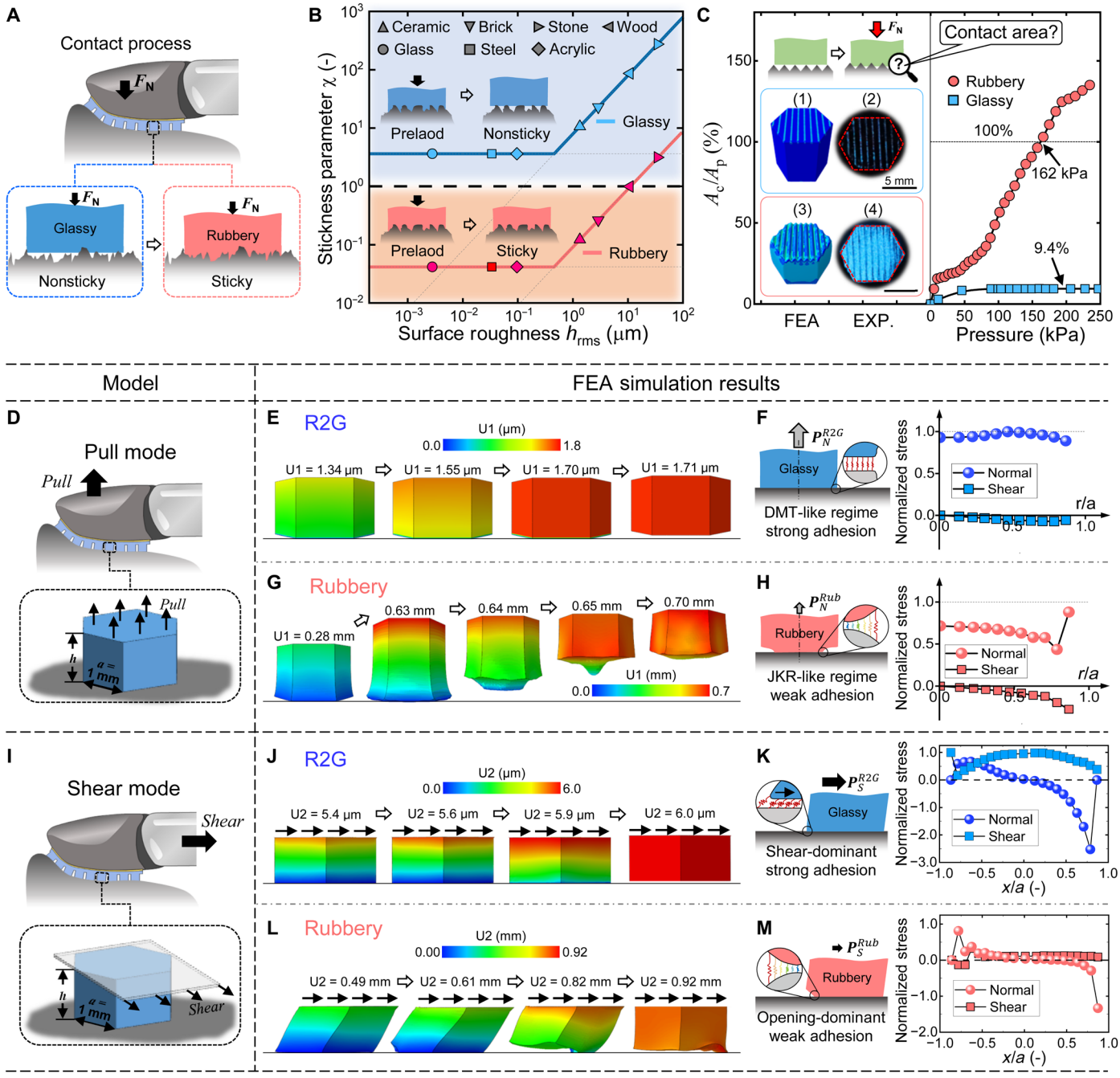

Fig. 3. Attachment/detachment mechanisms behind the SMP robotic skin. (**A** to **C**) Understanding on-demand attachment: (A) Illustrations showing nonsticky attachment in the glassy phase and sticky attachment in the rubbery phase. (B) Stickiness diagram for SMP adhesive fibrils ($a = 1$ mm; $h = 1$ mm) under zero preload, compared to typical adherend surface roughness (see details in section S6). The fibril is sticky ($\chi < 1$) in the rubbery phase and nonsticky ($\chi > 1$) in the glassy phase on most adherends. (C) Forced contact under preloads between an SMP adhesive fibril ($a = 5$ mm; $h = 10$ mm) and a steel substrate with a serrated surface. FEA results of the true contact area are normalized by the projected contact area as a function of preload pressure. Insets show the (1) and (3) FEA simulation results and (2) and (4) experimental observation of contact conditions in (1) and (2) glassy and (3) and (4) rubbery phases under a preload of 231 kPa. Both FEA and experimental results demonstrate that conformal contact is unachievable in the glassy phase but possible in the rubbery phase with sufficient preload (see details in sections S7 and S8). (**D** to **M**) FEA simulations of the detachment mechanisms of an SMP fibril ($a = 1$ mm; $h = 1$ mm). (D) Under the pull mode, the detachment shows (E) a uniform separation with (F) even normal stress distribution at the detachment point under the R2G condition but (G) a gradual crack propagation with (H) normal stress concentrated at the edge in the rubbery phase. (I) Under the shear mode, the detachment shows (J) a shear-dominant behavior with (K) shear stress dominated at the contact interface under the R2G condition but (L) an opening-dominant behavior (M) with normal stress dominating over the shear stress at the left crack front in the rubbery phase (see details in section S9).

nonsticky; a mesoscopic contact area cannot form, and the resulting adhesion force is negligible. On the other hand, for $\chi < 1$, the adhesive is sticky; a finite contact area forms even with minimal preload and an adhesion force is measurable during pull-off of the adhesive fibril from the adherend. Figure 3B shows that the SMP fibril in the glassy phase is nonsticky ($\chi > 1$) on all adherends. In the rubbery phase, the SMP fibril is sticky ($\chi < 1$) on most adherends with surface roughness (h_{rms}) up to 10.91 μm except for the highly roughened ($h_{rms} = 34.39$ μm) wooden surface.

The strongest adhesion on a rough substrate is achieved, of course, through R2G conditions. We further examined the contact behavior of a hexagonal SMP fibril (5 mm in edge length and 10 mm in height) with a highly roughened adherend like a segregated steel plate with 0.5-mm amplitude and 1-mm wavelength. Using the finite element analysis (FEA) (fig. S8 and section S7) and the contact testing with fluorescent coatings (fig. S9 and section S8), we find that conformal contact is possible under sufficiently high preload and can be maintained upon R2G transition due to the SMP's shape-locking effects (*48*). Figure 3C depicts the testing procedure and shows the ratio of the true contact area (A_c) to the projected contact area (A_p) on segregated adherend as a function of preload. It shows that, in the glassy phase, a small fraction (<10%) of the SMP surface is in contact with the adherend even at a preload of 250 kPa. The FEA (inset 1 in Fig. 3C) and fluorescent contact area image (inset 2 in Fig. 3C) confirm this result. In the rubbery phase, on the other hand, A_c increases with the preload, exceeding A_p when the preload is higher than 162 kPa and achieving conformal contact at a preload level of around 231 kPa (inset 3 from FEA and inset 4 from experimental data in Fig. 3C). These results demonstrate that the tunability of modulus and the shape-locking feature of the SMP play an essential role in enabling the adhesive skin to achieve on-demand attachment to various surfaces.

Another unique feature of the adhesive skin is its ability to easily switch from strong adhesion (approximately megapascal) to weak adhesion through the shape memory effect, characterized by the switchability ratio. Adhesion switchability is the ratio of the maximum adhesion strength to the minimum adhesion strength. The larger the switchability, the easier it is for the adhesive to transition from strong to weak adhesion and thus to detach on-demand. The SMP-based adhesion, under the R2G condition, exhibits a switchability ratio of more than 10^2 (fig. S3, C and D).

To understand the physical principle governing the detachment of the adhesive skin, we performed comprehensive FEA simulations of an adhesive SMP fibril ($a = 1$ mm; $h = 1$ mm) under pull or shear mode (fig. S10 and section S9). Under pull mode (Fig. 3D), the R2G adhesion behavior is DMT-like (*58*). The fibril detaches uniformly (Fig. 3E) when the interfacial normal stress reaches its theoretical limit and is evenly distributed across the contact interface (Fig. 3F), resulting in strong adhesion. In the rubbery phase, however, the SMP fibril detaches through crack propagation (Fig. 3G) when the energy release rate reaches the critical value and Griffith's criterion is met at the crack tip. This leads to an uneven load distribution across the contact interface and JKR-like adhesion (*58*) as shown in Fig. 3H, leading to reduced adhesion strength. Under shear mode (Fig. 3I), the detachment (Fig. 3J) and the interfacial stresses (Fig. 3K) are shear-dominant under the R2G condition. This results in a strong shear adhesion strength. In the rubbery phase, the SMP adhesive fibril displays an opening-dominant detachment behavior (Fig. 3L). Large deformation at the crack front or the edge causes the interfacial stress to be dominated by normal stress (Fig. 3M), resulting in weak shear adhesion strength. This opening-dominant failure under shear loading has also been reported in multilayer nanosheets (*69*).

Applications of SMP adhesive skins

As proof of concept, we integrated the adhesive skin onto a robotic hand and demonstrated that it can be used to perform various nonadhesive and adhesive functions. Figure 4A demonstrates that the adhesive skin integrated with a pressure sensor can detect surface morphology in the nonsticky, glassy phase. The nonadhesive state allows the robotic finger to slide smoothly across the surface with wavy textures of various amplitudes. Both the wavelength and amplitude of the recorded signals are consistent with surface textures. In contrast, when the SMP adhesive fibrils are in the sticky, rubbery phase or when the fibrils are made of polydimethylsiloxane (PDMS), the adhesion hinders accurate detection of the surface textures. Adhesion and stick-slip behavior (*47*, *70*, *71*) can cause significant noise as seen in the recorded signals (Fig. 4A and movie S1).

Similar challenges are encountered when the robotic hand is used to grip a light, 25-g towel to clean a plate (movie S2). After gripping the towel under the R2G conditions, the SMP is heated to the rubbery phase to reduce the adhesion, attempting to release the towel. However, in the sticky rubbery phase, even weak adhesion causes the towel to stick to the adhesive skin, preventing its release after cleaning (Fig. 4B). Neither opening nor shaking of the robotic fingers could release the towel due to adhesion. In contrast, when gripping in the nonsticky, glassy phase, the frictional force from the fingers allowed reliable pickup of the towel for cleaning (Fig. 4C) and easy release by opening the grips.

Using the adhesive skin's ability to attach with high adhesion strength under the R2G condition and detach with low adhesion strength in the rubbery phase, we demonstrate the on-demand, switchable adhesion for various robotic manipulations. For example, robotic fingers mounted with the adhesive skin can grip and release fragile quail eggs (Fig. 5A and movie S3). Frictional gripping of an object typically requires sufficiently high pressure (as in the case of human hand picking up a glass of water), and the ultrastrong R2G adhesion allows the robotic fingers to grip quail egg with minimal preload. The large grip force to preload ratio (>50) ensures that the quail eggs adhere firmly to the robotic fingers and are released easily when the adhesive skin is reheated to the rubbery phase. Figure 5A also demonstrates the robotic hand's ability to manipulate multiple quail eggs simultaneously. In contrast, conventional rigid grippers are prone to breaking the eggs during manipulation (*72*).

Because the SMP adhesion is based on physical, van der Waals interactions, and the shape-locking effect, it is ubiquitous, not depending on the adherend materials or surface conditions. Figure 5B and movie S4 demonstrate that robotic hands with adhesive skin can grip objects made of various materials including plastics, wood, glass, and ceramics, as well as objects with different surface curvatures, from hollow steel balls with radius ranging from 10 to 40 cm to flat glass plates. In contrast, without the adhesive skin, the robotic hand is unable to grip even a relatively small steel ball with a radius of 10 cm (fig. S11 and section S10). Mounting the adhesive skin on an electronic glove also allows a person to pick up multiple objects simultaneously or handle large and smooth steel balls (fig. S12 and section S11).

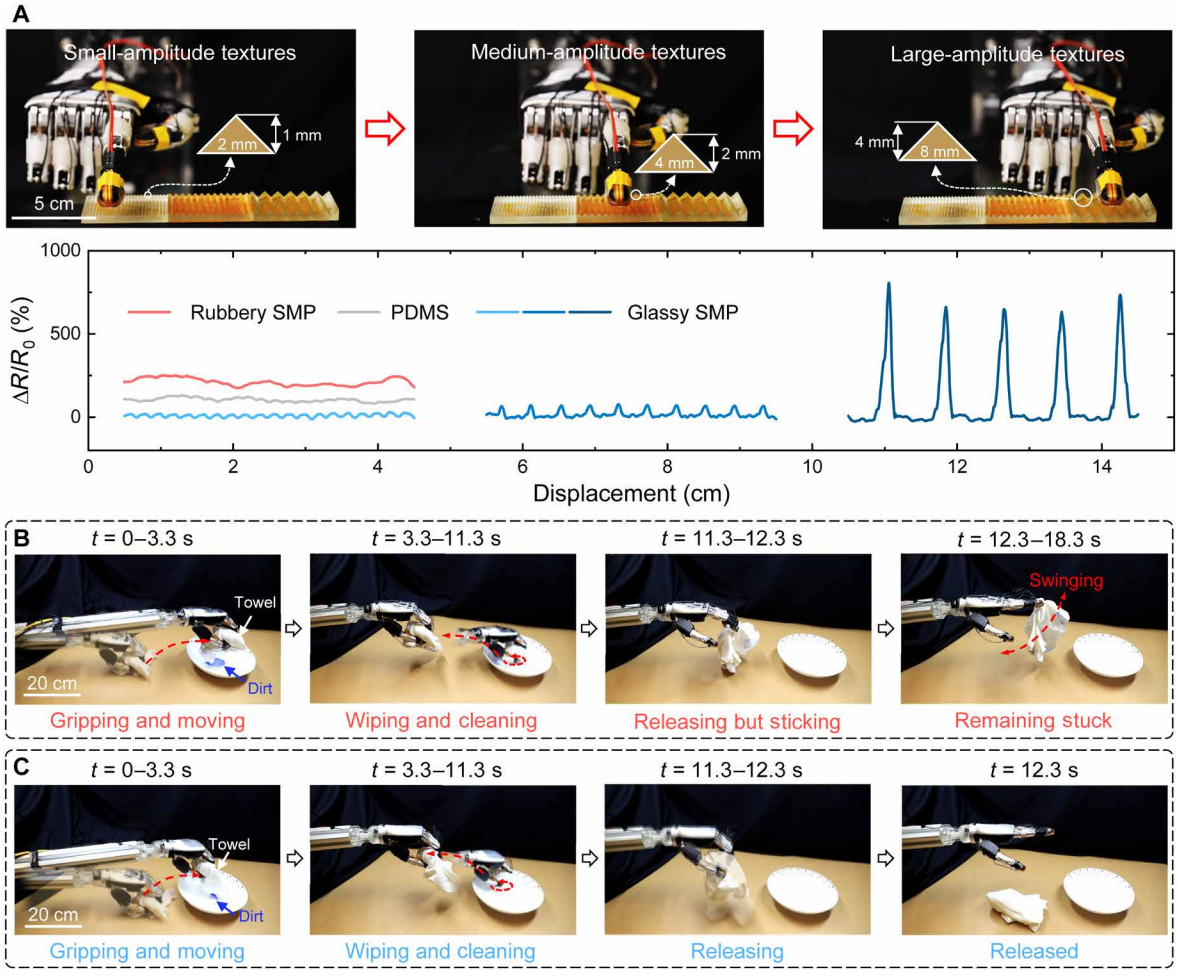

Fig. 4. Demonstrations of applications using the integrated robotic adhesive skin system in its nonsticky state. (**A**) Surface morphology detection, where minimal adhesion between the substrate and SMP fibrils in the glassy phase enables smooth traversal of the robotic hand across various surface textures with small, medium, and large amplitudes, resulting in accurate detection of surface morphologies using a pressure sensor (blue lines). In contrast, for PDMS or SMP fibrils in the rubbery phase, accurate detection of the surface morphologies is hindered, and the recorded signals (red line for rubbery SMP and gray line for PDMS) exhibit a lot of noise caused by adhesion and stick-slip issues (see more details in movie S1). (**B** and **C**) Handling a light object, where a towel (25 g) is used for cleaning a plate. (B) Upon contact in the rubbery phase, the sticky SMP skin on robotic fingers obstructs the release process after gripping, wiping, and cleaning manipulations. (C) In contrast, in the glassy phase, the frictional force facilitates reliable gripping and manipulations (wiping and cleaning), and the minimal adhesion ensures an instantaneous release upon opening the robotic fingers (see more details in movie S2). "*t*" in (B) and (C) refer to the time. s, seconds.

The ability of a friction-based robotic gripper to pick up an object is limited by the amount of pressure the object can bear or by the load capacity of the robotic motor. Figure 5C and movie S5 show that a robotic hand trying to grip a heavy (1.2 kg) aluminum block with adhesive skin in the glassy phase slips and fails due to insufficient friction. In contrast, Fig. 5D and movie S5 show a robotic hand with adhesive skin under the R2G condition ensures the firm gripping and lifting of the aluminum block and easy release of it when heated back to the rubbery phase. In summary, these demonstrations show that the SMP-based adhesive skin, under the R2G condition, has the potential to greatly enhance the efficiency and capabilities of robots.

DISCUSSION

In this study, we successfully engineered a versatile robotic adhesive skin by integrating SMP adhesive fibrils, flexible heaters, and flexible pressure sensors. The adhesive skin exhibits both the sensory functions of natural skin tissues and the on-demand adhesive capabilities. The tunable properties of SMPs enable the adhesive skin to attach strongly to and detach easily from a wide range of material surfaces. We show that with the adhesive skin, a robotic hand can manipulate a variety of objects in ways that existing adhesives cannot. The adhesive skin can also be used in various scenarios, from accurately detecting surface textures and dexterous handling of lightweight items to securely gripping fragile, large, or heavy objects. The adhesive skin greatly expands the scope and capabilities of interactions that are available to robots in diverse environments, including those where adhesion is desired or to be avoided.

Our adhesive skin with its broad adhesion spectrum (0.65 kPa to 2 MPa in pull mode and 2.86 kPa to 5.1 MPa in shear mode) and large adhesion switchability (>100) under ultrastrong adhesion strength (>1 MPa) is expected to reshape industries that require precise and adaptable object manipulation. In measurement, maintenance,

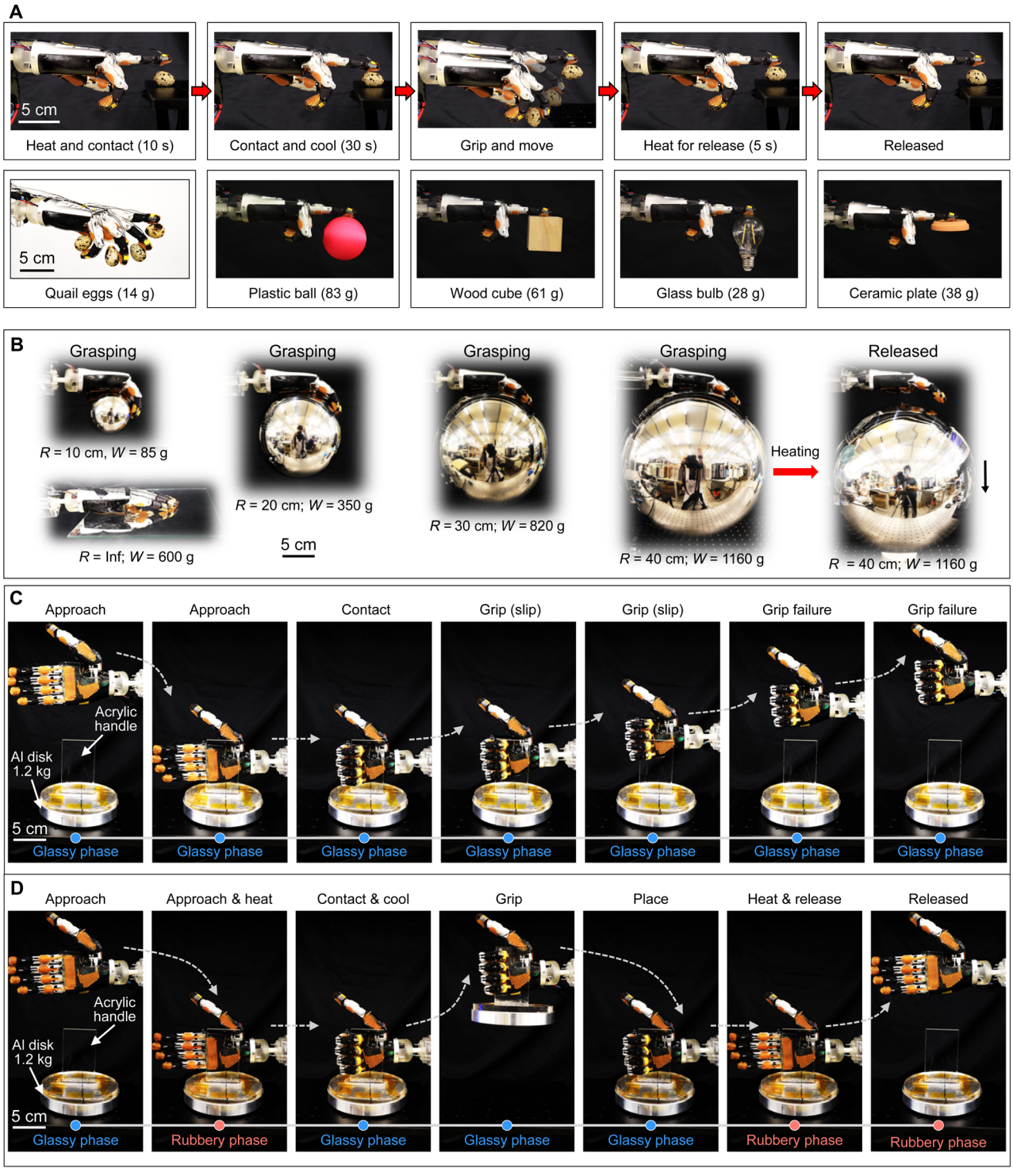

Fig. 5. Demonstrations of applications using the integrated robotic adhesive skin system in its switchable adhesion state. (**A**) Gripping of various kinds of objects, including quail eggs, plastic ball, wood cube, glass bub, and ceramic plate. (**B**) Gripping and release of large objects, including steel shells with radii ranging from 10 to 40 cm, and a flat glass plate. (**C** and **D**) Comparison of gripping manipulations of a heavy aluminum disk (1.2 kg) with an acrylic handle using the robotic hand equipped with SMP adhesive skins in the (C) glassy phase relying on friction, which cannot provide sufficient gripping force and leads to sliding and gripping failure, versus (D) the reliable gripping via strong R2G adhesion followed by release in the rubbery phase. s, seconds.

textile, and paper industries, where surface detection and dexterous manipulation are crucial, this robotic technology promises to enhance productivity, safety, and precision by providing good adhesion and preventing unwanted adhesion on-demand. In manufacturing, the robots' ability to precisely handle fragile and delicate components with switchable adhesion can improve product quality and production efficiency. Whereas in industries such as construction and logistics, this robotic technology can provide strong and robust adhesive for securely grasping heavy objects and deliver the cargos to target locations. In health care, robots with adhesive E-skin can be used for delicate and precise operations with minimal risks to patients. Successful integration of these adhesive skins into electronic adhesive gloves also highlights their potential to enhance our ability to perform daily activities that are deemed too difficult.

For practical applications, however, the switching speed between the rubbery and glassy phases will need to be optimized. The current thermal control mechanism, which takes about 1 min for a heating and cooling cycle, is slow for some applications that require the adhesive to attach and detach rapidly. In addition, the transition temperature is around 51°C, which limits the robotic skin's applicability in temperature-sensitive scenarios, such as handling humans or live animals. Alternative materials with faster transitions (*73*–*76*) that might involve different actuation methods and lower transition temperatures (*77*) may be explored in future studies. On the other hand, for high-temperature applications, SMPs with higher transition temperature should be applied. Integrating other types of sensors onto the adhesive skin to match or exceed the capabilities of natural skin would broaden its applications. Furthermore, incorporating communication capabilities into these sensors can enhance the versatility of the adhesive skins even more. For example, detected signals can be used to guide the amount of preload applied during gripping. In addition, further exploration of the arrangement and interaction between sensors, adhesive layers, flexible heaters, and pillars is needed to improve sensing capabilities. Thermal isolation designs should also be incorporated to accommodate both flexible heaters and temperature sensors. The shape and arrangement of the adhesive fibrils, as well as the curvature effects of the skins, can be further optimized to achieve better adhesion capabilities. Having a single adhesive that can attach and detach on-demand for various application scenarios is an important step forward in the field of robotics because it extends the range of interactions a robot can have with its environment.

MATERIALS AND METHODS

Materials

Clear Resin (Formlabs Inc., USA) was used for the stiff molding. Ecoflex 00-30 (Smooth-On Inc., USA) was used for soft molding. The E44 monomer (Feicheng Deyuan Chemical Co., China) and the cross-linker poly(propyleneglycol)bis(2-aminopropylether) (Shanghai Aladdin Bio-Chem Technology Co. Ltd., China) were used to fabricate the adhesive skin. Flexible printed circuit board heaters were ordered from Shenzhen Huaxin Express Technology Co. Ltd., China, and the flexible piezoresistive pressure sensors were ordered from Shanghai CHENG TEC Co. Ltd., China.

Methods

Fabrication of the adhesive skin patches

We started the production of the adhesive skin patches by creating a stiff mold with pillar arrays, fabricated using Clear Resin and a Form 3+ SLA 3D printer. Ecoflex 00-30 precursors were mixed in equal parts, degassed for 3 min, and poured into the mold, followed by another 5-min degassing. The mix was cured at room temperature for 2 hours, forming a soft Ecoflex mold with pillar holes. Liquid adhesive precursors were then cast into this soft mold, with a flexible heater embedded in the liquid. Following a final degassing, the mixture was left to cure, resulting in adhesive skin patches with top fibrillar structures and integrated flexible heaters. These patches, designed for various positions of a robotic hand including fingers and palm areas, were tailored according to the dimensions of the rigid molds. More details can be found in section S1.

Synthesis of the E-44 SMP

The E44-SMP was prepared by mixing the liquid cross-linker, poly(propyleneglycol)bis(2-aminopropylether), with the liquid E44 monomer at a mass ratio of 81:48. Subsequently, this mixture underwent a 30-min degassing process in a vacuum chamber. Following the degassing, the liquid compound was poured into molds and subjected to a 2-hour precuring phase at 50°C. This was followed by 1 hour of curing at 100°C and a subsequent postcuring period of 1 hour at 130°C. More details can be found in section S2.

Modulus characterization of the E44-SMP

A dynamic mechanical analyzer was used to assess the storage modulus (E') of the SMP materials across a range of temperatures, using a measuring frequency of 0.5 Hz and a temperature ramp rate of 2°C/min. To produce the rectangular test specimens (each measuring 30 mm in length, 6 mm in width, and 2 mm in thickness), we formed an initial 2-mm-thick SMP membrane within the mold. Subsequently, these specimens were precision cut into the desired geometry using a laser cutter. More details can be found in section S2.

Fabrication of the rough SMP adhesive fibrils

The rough surface textures of the SMP adhesive fibril tips were replicated from sandpapers. Initially, a rigid fibril mold was generated via 3D printing, onto which a sandpaper template was affixed. Subsequently, liquid Ecoflex precursors, which had been mixed and degassed in advance, were poured into the rigid mold. Following a 2-hour curing period at room temperature, the pliable Ecoflex mold was acquired. Next, premixed and degassed SMP liquid precursors were introduced into the flexible Ecoflex mold and subjected to an additional 30-min degassing process in a vacuum chamber. Ultimately, the resulting SMP rough fibril, reproducing the surface texture of the sandpaper template, was obtained following curing in an oven (further details can be found in section S4).

Adhesion test of the SMP adhesive fibrils

Pull-off tests (*48*, *58*) were used to quantify the normal adhesion behavior. During these tests, the adhesive samples were gently brought into contact with the glass adherend surface at an extremely low speed of 10 μm/s. Subsequently, they were steadily pulled away at a constant speed of 10 mm/min, controlled by displacement. The shear adhesion performance was assessed using shearing tests. In this procedure, SMP adhesive fibrils, attached to a glass indenter, were linked to a vertical load cell via a clamp. This setup enabled the controlled contact of the SMP fibrils with a sliding glass placed on a stationary glass, achieved by moving the vertical load cell at a speed of 10 μm/s until a predetermined preload was reached. Subsequently, the horizontal load cell, through a connecting string, laterally sheared the sliding glass at 10 mm/min. The resulting shear adhesion force was determined by calibrating against the frictional force between the moving and stationary glass substrates. Additional information is provided in section S5 for reference.

Calculation of the stickness parameter

The stickiness parameter (*68*) was given as $\chi = \left(h_{\mathrm{rms}}/\varepsilon\right) / \left(\frac{9}{4}\frac{l_a/\varepsilon}{\varepsilon q_0}\right)^{0.6}$, where $h_{\mathrm{rms}} = \mathrm{Max}\left(h^{\mathrm{f}}_{\mathrm{rms}}, h^{\mathrm{a}}_{\mathrm{rms}}\right)$ is the maximum RMS roughness amplitude among the SMP adhesive fibril $h^{\mathrm{f}}_{\mathrm{rms}}$ and the adherend $h^{\mathrm{a}}_{\mathrm{rms}}$, and $\varepsilon = \Delta\gamma/\sigma_{\mathrm{th}}$ is the adhesive interaction distance with $\Delta\gamma$ being the work of adhesion and σ_{th} as the theoretical adhesion strength, $l_{\mathrm{a}} = \Delta\gamma/E^*$ defines a characteristic adhesion length that can be used to quantify the relative strength of adhesion, where $E^* = E/\left(1-\nu^2\right)$ with E and ν being the modulus and Poisson's ratio of the SMP adhesive fibril, respectively; $q_0 = 2\pi/L$ is the largest wavelength in the roughness spectrum with L as the largest lateral characteristic dimension. For van der Waals force (*78*), $\varepsilon \sim 10^{-9}$ m and $\Delta\gamma \sim 10$ mJ/m^2. For the SMP adhesive fibril, $L = 2$ mm, leading to $\varepsilon q_0 \sim \pi \times 10^{-6}$. The modulus values of the SMP are 1 MPa and 2 GPa, and Poisson's ratios are 0.5 and 0.35, in the rubbery and glassy phases, respectively.

FEA simulations of the forced contact

Three-dimensional (3D) FEA simulations using ABAQUS were carried out to examine the forced contact between a hexagonal SMP fibril and a segregated steel plate in both rubbery and glassy phases. The simulation involved a square die compressing the SMP fibril against the plate, both assumed to be much stiffer than the SMP. The rubbery phase of the SMP was modeled using the first-order Ogden-Roxburgh model, whereas the glassy phase was modeled as an isotropic elastic solid. Displacement boundary conditions were applied in the simulations, with the bottom plate fixed and a given displacement loading at a velocity of 1 mm/s applied on the die. The FEA used coupled Eulerian-Lagrangian analysis, with the SMP fibrils and the die/plate modeled using Eulerian and Lagrangian elements, respectively. The contact pressure images were processed using ImageJ to determine the contact area under different pressures. See more details in section S7.

Experimental observation of the forced contact

Macroscopic contact tests were performed to evaluate the SMP's attachment capabilities during its phase transition from glassy to rubbery. The tests used a hexagonal SMP fibril molded to specific dimensions (edge length = 5 mm and height = 10 mm) and a machined segregated steel plate (amplitude = 0.5 mm and wavelength = 1 mm). Fluorescent nanoparticles, illuminating under ultraviolet (UV) light, were used to mark the contact areas. The process involved coating the substrate with a PDMS layer for nanoparticle adhesion, followed by the application of the nanoparticles and subsequent removal of excess nanoparticles. The contact procedure varied with the SMP's phase. In the glassy phase, the SMP fibril's contact with the nanoparticle-laden substrate facilitated nanoparticle transfer. These contact regions were then illuminated with UV light and imaged in the dark. Similarly, in the rubbery phase, the SMP's shape locking upon reverting to the glassy phase maintained the contact pattern, which was also visualized post-UV irradiation in a dark room. See details in section S8.

FEA simulations of on-demand detachment

3D FEA simulations were performed in ABAQUS/Explicit to analyze the switchable adhesion of SMP adhesive fibrils under both pull and shear modes. In the pull mode, vertical pulling displacement was applied to the top of the SMP fibril. In the shear mode, shear displacements were applied to a rigid plate tied to the fibril's upper surface. The adhesion was modeled using a layer of cohesive elements with zero thickness. C3D8R elements were used for the SMP fibril, and COH3D8 elements for the cohesive layer, with a 50-μm mesh size. The SMP was modeled as an elastic material with a modulus of 2 GPa and a Poisson's ratio of 0.35 in its glassy phase and as a hyperelastic material described by the Ogden model in its rubbery phase. Adhesive interactions were modeled using a linear traction–separation law, with damage initiation and evolution parameters specified for both pull and shear modes as detailed in section S9 in the Supplementary Materials. The FEA explored four scenarios: pull and shear modes in both rubbery and glassy phases. These processes involved applying displacements until the SMP fibril detached. See more details in section S9 in the Supplementary Materials.

Supplementary Materials

The PDF file includes:

Supplementary Sections S1 to S11
Figs. S1 to S12
Tables S1 and S2
Legends for movies S1 to S5
References

Other Supplementary Material for this manuscript includes the following:

Movies S1 to S5

REFERENCES AND NOTES

1. W. Montagna, *The Structure and Function of Skin* (Elsevier, 2012).
2. R. K. Freinkel, D. T. Woodley, *The Biology of the Skin* (CRC Press, 2001).
3. E. Arzt, H. Quan, R. M. McMeeking, R. Hensel, Functional surface microstructures inspired by nature—From adhesion and wetting principles to sustainable new devices. *Prog. Mater. Sci.* **120**, 100823 (2021).
4. M. Scherge, S. Gorb, *Biological Micro- and Nanotribology* (Springer Science & Business Media, 2001).
5. A. M. Smith, J. A. Callow, *Biological Adhesives* (Springer, 2006), vol. 23.
6. H. Cho, G. Wu, J. Christopher Jolly, N. Fortoul, Z. He, Y. Gao, A. Jagota, S. Yang, Intrinsically reversible superglues via shape adaptation inspired by snail epiphragm. *Proc. Natl. Acad. Sci. U.S.A.* **116**, 13774–13779 (2019).
7. Y. Wang, X. Yang, Y. Chen, D. K. Wainwright, C. P. Kenaley, Z. Gong, Z. Liu, H. Liu, J. Guan, T. Wang, J. C. Weaver, R. J. Wood, L. Wen, A biorobotic adhesive disc for underwater hitchhiking inspired by the remora suckerfish. *Sci. Robot.* **2**, eaan8072 (2017).
8. L. Li, S. Wang, Y. Zhang, S. Song, C. Wang, S. Tan, W. Zhao, G. Wang, W. Sun, F. Yang, J. Liu, B. Chen, H. Xu, P. Nguyen, M. Kovac, L. Wen, Aerial-aquatic robots capable of crossing the air-water boundary and hitchhiking on surfaces. *Sci. Robot.* **7**, eabm6695 (2022).
9. F. Brau, D. Lanterbecq, L.-N. Zghikh, V. Bels, P. Damman, Dynamics of prey prehension by chameleons through viscous adhesion. *Nat. Phys.* **12**, 931–935 (2016).
10. Z. Xie, F. Yuan, J. Liu, L. Tian, B. Chen, Z. Fu, S. Mao, T. Jin, Y. Wang, X. He, G. Wang, Y. Mo, X. Ding, Y. Zhang, C. Laschi, L. Wen, Octopus-inspired sensorized soft arm for environmental interaction. *Sci. Robot.* **8**, eadh7852 (2023).
11. M. Cianchetti, M. Calisti, L. Margheri, M. Kuba, C. Laschi, Bioinspired locomotion and grasping in water: The soft eight-arm OCTOPUS robot. *Bioinspir. Biomim.* **10**, 035003 (2015).
12. D. Labonte, C. J. Clemente, A. Dittrich, C. Y. Kuo, A. J. Crosby, D. J. Irschick, W. Federle, Extreme positive allometry of animal adhesive pads and the size limits of adhesion-based climbing. *Proc. Natl. Acad. Sci. U.S.A.* **113**, 1297–1302 (2016).
13. A. Peattie, R. Full, Phylogenetic analysis of the scaling of wet and dry biological fibrillar adhesives. *Proc. Natl. Acad. Sci. U.S.A.* **104**, 18595–18600 (2007).
14. E. Arzt, S. Gorb, R. Spolenak, From micro to nano contacts in biological attachment devices. *Proc. Natl. Acad. Sci. U.S.A.* **100**, 10603–10606 (2003).
15. W. G. Bircher, A. S. Morgan, A. M. Dollar, Complex manipulation with a simple robotic hand through contact breaking and caging. *Sci. Robot.* **6**, eabd2666 (2021).
16. U. Kim, D. Jung, H. Jeong, J. Park, H. M. Jung, J. Cheong, H. R. Choi, H. Do, C. Park, Integrated linkage-driven dexterous anthropomorphic robotic hand. *Nat. Commun.* **12**, 7177 (2021).
17. J. Mahler, M. Matl, V. Satish, M. Danielczuk, B. DeRose, S. McKinley, K. Goldberg, Learning ambidextrous robot grasping policies. *Sci. Robot.* **4**, eaau4984 (2019).
18. S. Kim, J. Wu, A. Carlson, S. H. Jin, A. Kovalsky, P. Glass, Z. Liu, N. Ahmed, S. L. Elgan, W. Chen, P. M. Ferreira, M. Sitti, Y. Huang, J. A. Rogers, Microstructured elastomeric surfaces with reversible adhesion and examples of their use in deterministic assembly by transfer printing. *Proc. Natl. Acad. Sci. U.S.A.* **107**, 17095–17100 (2010).
19. C. Linghu, C. Wang, N. Cen, J. Wu, Z. Lai, J. Song, Rapidly tunable and highly reversible bio-inspired dry adhesion for transfer printing in air and a vacuum. *Soft Matter* **15**, 30–37 (2019).

20. J. Zhao, X. Li, Y. Tan, X. Liu, T. Lu, M. Shi, Smart adhesives via magnetic actuation. *Adv. Mater.* **34**, 2107748 (2022).
21. X. Liu, Y. Cao, K. Zheng, Y. Zhang, Z. Wang, Y. Chen, Y. Chen, Y. Ma, X. Feng, Liquid droplet stamp transfer printing. *Adv. Funct. Mater.* **31**, 2105407 (2021).
22. S. Zhang, H. Luo, S. Wang, Z. Chen, S. Nie, C. Liu, J. Song, A thermal actuated switchable dry adhesive with high reversibility for transfer printing. *Int. J. Extrem Manuf.* **3**, 035103 (2021).
23. C. Linghu, S. Zhang, C. Wang, J. Song, Transfer printing techniques for flexible and stretchable inorganic electronics. *Npj Flex. Electron.* **2**, 26 (2018).
24. F. Chen, M. Gai, N. Sun, Z. Xu, L. Liu, H. Yu, J. Bian, Y. A. Huang, Laser-driven hierarchical "gas-needles" for programmable and high-precision proximity transfer printing of microchips. *Sci. Adv.* **9**, eadk0244 (2023).
25. H. Liu, H. Tian, D. Wang, T. Yuan, J. Zhang, G. Liu, X. Li, X. Chen, C. Wang, S. Cai, J. Shao, Electrically active smart adhesive for a perching-and-takeoff robot. *Sci. Adv.* **9**, eadj3133 (2023).
26. Y. W. Lee, S. Chun, D. Son, X. Hu, M. Schneider, M. Sitti, A tissue adhesion-controllable and biocompatible small-scale hydrogel adhesive robot. *Adv. Mater.* **34**, 2109325 (2022).
27. E. Brown, N. Rodenberg, J. Amend, A. Mozeika, E. Steltz, M. R. Zakin, H. Lipson, H. M. Jaeger, Universal robotic gripper based on the jamming of granular material. *Proc. Natl. Acad. Sci. U.S.A.* **107**, 18809–18814 (2010).
28. C. Linghu, S. Zhang, C. Wang, K. Yu, C. Li, Y. Zeng, H. Zhu, X. Jin, Z. You, J. Song, Universal SMP gripper with massive and selective capabilities for multiscaled, arbitrarily shaped objects. *Sci. Adv.* **6**, eaay5120 (2020).
29. D. J. Levine, G. M. Iyer, R. Daelan Roosa, K. T. Turner, J. H. Pikul, A mechanics-based approach to realize high–force capacity electroadhesives for robots. *Sci. Robot.* **7**, eabo2179 (2022).
30. H. Jiang, E. W. Hawkes, C. Fuller, M. A. Estrada, S. A. Suresh, N. Abcouwer, A. K. Han, S. Wang, C. J. Ploch, A. Parness, M. R. Cutkosky, A robotic device using gecko-inspired adhesives can grasp and manipulate large objects in microgravity. *Sci. Robot.* **2**, eaan4545 (2017).
31. W. Ruotolo, D. Brouwer, M. R. Cutkosky, From grasping to manipulation with gecko-inspired adhesives on a multifinger gripper. *Sci. Robot.* **6**, eabi9773 (2021).
32. B. Shih, D. Shah, J. Li, T. G. Thuruthel, Y. L. Park, F. Iida, Z. Bao, R. Kramer-Bottiglio, M. T. Tolley, Electronic skins and machine learning for intelligent soft robots. *Sci. Robot.* **5**, eaaz9239 (2020).
33. F. Liu, S. Deswal, A. Christou, Y. Sandamirskaya, M. Kaboli, R. Dahiya, Neuro-inspired electronic skin for robots. *Sci. Robot.* **7**, eabl7344 (2022).
34. Y. Yu, J. Li, S. A. Solomon, J. Min, J. Tu, W. Guo, C. Xu, Y. Song, W. Gao, All-printed soft human-machine interface for robotic physicochemical sensing. *Sci. Robot.* **7**, eabn0495 (2022).
35. Y. H. Jung, J. Y. Yoo, A. Vázquez-Guardado, J. H. Kim, J. T. Kim, H. Luan, M. Park, J. Lim, H. S. Shin, C. J. Su, R. Schloen, J. Trueb, R. Avila, J. K. Chang, D. S. Yang, Y. Park, H. Ryu, H. J. Yoon, G. Lee, H. Jeong, J. U. Kim, A. Akhtar, J. Cornman, T. I. Kim, Y. Huang, J. A. Rogers, A wireless haptic interface for programmable patterns of touch across large areas of the skin. *Nat. Electron.* **5**, 374–385 (2022).
36. D.-H. Kim, N. Lu, R. Ma, Y. S. Kim, R. H. Kim, S. Wang, J. Wu, S. M. Won, H. Tao, A. Islam, K. J. Yu, T. I. Kim, R. Chowdhury, M. Ying, L. Xu, M. Li, H. J. Chung, H. Keum, M. McCormick, P. Liu, Y. W. Zhang, F. G. Omenetto, Y. Huang, T. Coleman, J. A. Rogers, Epidermal electronics. *Science* **333**, 838–843 (2011).
37. F. Chen, Q. Zhuang, Y. Ding, C. Zhang, X. Song, Z. Chen, Y. Zhang, Q. Mei, X. Zhao, Q. Huang, Z. Zheng, Wet-adaptive electronic skin. *Adv. Mater.* **35**, e2305630 (2023).
38. J. C. Yang, J. Mun, S. Y. Kwon, S. Park, Z. Bao, S. Park, Electronic skin: Recent progress and future prospects for skin-attachable devices for health monitoring, robotics, and prosthetics. *Adv. Mater.* **31**, e1904765 (2019).
39. G. Yao, L. Xu, X. Cheng, Y. Li, X. Huang, W. Guo, S. Liu, Z. L. Wang, H. Wu, Bioinspired triboelectric nanogenerators as self-powered electronic skin for robotic tactile sensing. *Adv. Funct. Mater.* **30**, 1907312 (2020).
40. K. Sim, Z. Rao, Z. Zou, F. Ershad, J. Lei, A. Thukral, J. Chen, Q. A. Huang, J. Xiao, C. Yu, Metal oxide semiconductor nanomembrane–based soft unnoticeable multifunctional electronics for wearable human-machine interfaces. *Sci. Adv.* **5**, eaav9653 (2019).
41. M. Cianchetti, C. Laschi, A. Menciassi, P. Dario, Biomedical applications of soft robotics. *Nat. Rev. Mater.* **3**, 143–153 (2018).
42. G. Gu, N. Zhang, H. Xu, S. Lin, Y. Yu, G. Chai, L. Ge, H. Yang, Q. Shao, X. Sheng, X. Zhu, X. Zhao, A soft neuroprosthetic hand providing simultaneous myoelectric control and tactile feedback. *Nat. Biomed. Eng.* **7**, 589–598 (2023).
43. D. C. Rose, J. Lyon, A. de Boon, M. Hanheide, S. Pearson, Responsible development of autonomous robotics in agriculture. *Nat. Food* **2**, 306–309 (2021).
44. J. Cui, J. Trinkle, Toward next-generation learned robot manipulation. *Sci. Robot.* **6**, eabd9461 (2021).
45. C. Laschi, B. Mazzolai, M. Cianchetti, Soft robotics: Technologies and systems pushing the boundaries of robot abilities. *Sci. Robot.* **1**, eaah3690 (2016).
46. K. Kendall, in *Molecular Adhesion and Its Applications: The Sticky Universe* (Springer US, 2001), pp. 3–23.
47. Z. Zhang, C. Qin, H. Feng, Y. Xiang, B. Yu, X. Pei, Y. Ma, F. Zhou, Design of large-span stick-slip freely switchable hydrogels via dynamic multiscale contact synergy. *Nat. Commun.* **13**, 6964 (2022).
48. C. Linghu, Y. Liu, Y. Y. Tan, J. H. M. Sing, Y. Tang, A. Zhou, X. Wang, D. Li, H. Gao, K. J. Hsia, Overcoming the adhesion paradox and switchability conflict on rough surfaces with shape-memory polymers. *Proc. Natl. Acad. Sci. U.S.A.* **120**, e2221049120 (2023).
49. Y. Wang, X. Zhang, R. Hensel, E. Arzt, Sliding mechanism for release of superlight objects from micropatterned adhesives. *Adv. Mater. Interfaces* **9**, 2101764 (2022).
50. H. Yin, A. Varava, D. Kragic, Modeling, learning, perception, and control methods for deformable object manipulation. *Sci. Robot.* **6**, eabd8803 (2021).
51. H. Zhao, K. O'Brien, S. Li, R. F. Shepherd, Optoelectronically innervated soft prosthetic hand via stretchable optical waveguides. *Sci. Robot.* **1**, eaai7529 (2016).
52. S. Sundaram, P. Kellnhofer, Y. Li, J. Y. Zhu, A. Torralba, W. Matusik, Learning the signatures of the human grasp using a scalable tactile glove. *Nature* **569**, 698–702 (2019).
53. H. Yao, W. Yang, W. Cheng, Y. J. Tan, H. H. See, S. Li, H. P. A. Ali, B. Z. H. Lim, Z. Liu, B. C. K. Tee, Near–hysteresis-free soft tactile electronic skins for wearables and reliable machine learning. *Proc. Natl. Acad. Sci. U.S.A.* **117**, 25352–25359 (2020).
54. J. Eisenhaure, S. Kim, High-strain shape memory polymers as practical dry adhesives. *Int. J. Adhes. Adhes.* **81**, 74–78 (2018).
55. N. Zheng, G. Fang, Z. Cao, Q. Zhao, T. Xie, High strain epoxy shape memory polymer. *Poly. Chem.* **6**, 3046–3053 (2015).
56. Y. Zhang, X. Wan, X. Xu, P. Teng, S. Wang, Recent progress of tree frog toe pads inspired wet adhesive materials. *Biosurf. Biotribol.* **8**, 279–289 (2022).
57. Y. Guo, L. Zhang, Y. Wang, J. Liang, X. Liu, Y. Jiang, L. Jiang, H. Chen, Nanofiber embedded bioinspired strong wet friction surface. *Sci. Adv.* **9**, eadi4843 (2023).
58. C. Linghu, X. Yang, Y. Liu, D. Li, H. Gao, K. J. Hsia, Mechanics of shape-locking-governed R2G adhesion with shape memory polymers. *J. Mech. Phys. Solids* **170**, 105091 (2023).
59. D. Tan, X. Wang, Q. Liu, K. Shi, B. Yang, S. Liu, Z. S. Wu, L. Xue, Switchable adhesion of micropillar adhesive on rough surfaces. *Small* **15**, e1904248 (2019).
60. S. H. Lee, H. W. Song, H. J. Park, M. K. Kwak, Surface adaptable and adhesion controllable dry adhesive with shape memory polymer. *Macromol. Rapid Commun.* **43**, e2200012 (2022).
61. J. D. Eisenhaure, S. Il Rhee, A. M. al-Okaily, A. Carlson, P. M. Ferreira, Seok Kim, The use of shape memory polymers for microassembly by transfer printing. *J. Microelectromech. Syst.* **23**, 1012–1014 (2014).
62. J. K. Park, J. D. Eisenhaure, S. Kim, Reversible underwater dry adhesion of a shape memory polymer. *Adv. Mater. Interfaces* **6**, 1801542 (2019).
63. S. Zhuo, Z. Zhao, Z. Xie, Y. Hao, Y. Xu, T. Zhao, H. Li, E. M. Knubben, L. Wen, L. Jiang, M. Liu, Complex multiphase organohydrogels with programmable mechanics toward adaptive soft-matter machines. *Sci. Adv.* **6**, eaax1464 (2020).
64. Y. Li, X. Liu, R. Wang, S. Jiao, Y. Liu, H. Lai, Z. Cheng, Triple-bioinspired shape memory microcavities with strong and switchable adhesion. *ACS Nano* **17**, 23595–23607 (2023).
65. C. Linghu, Y. Liu, X. Yang, D. Li, Y. Y. Tan, M. H. B. Mohamed Hafiz, M. F. B. Rohani, Z. du, J. Su, Y. Li, Y. Huo, H. Xu, X. Wang, Y. Wang, J. Yu, H. Gao, K. J. Hsia, Fibrillar adhesives with unprecedented adhesion strength, switchability and scalability. *Natl. Sci. Rev.* **11**, nwae106 (2024).
66. M. Seong, I. Hwang, S. Park, H. Jang, G. Choi, J. Kim, S. K. Kim, G. H. Kim, J. Yeo, H. E. Jeong, Enhanced thermal transport across self-interfacing van der Waals contacts in flexible thermal devices. *Adv. Funct. Mater.* **31**, 2107023 (2021).
67. C. Linghu, Z. Du, Y. Sun, W. Chen, K. J. Hsia, On shear adhesion of adhesive fibrils. *Extreme Mech. Lett.* **64**, 102092 (2023).
68. G. Violano, L. Afferrante, A. Papangelo, M. Ciavarella, On stickiness of multiscale randomly rough surfaces. *J. Adhes.* **97**, 509–527 (2021).
69. C. J. Castilho, D. Li, Y. Xie, H. Gao, R. H. Hurt, Shear failure in supported two-dimensional nanosheet van der Waals thin films. *Carbon* **173**, 410–418 (2021).
70. Y. Roh, S. Lee, S. M. Won, S. Hwang, D. Gong, C. Kim, I. Hong, D. Lim, H. Kim, M. Kim, B. Kim, T. Kim, S. Im, D. Shin, U. Kim, J. Choi, J. S. Koh, D. Kang, S. Han, Crumple-recoverable electronics based on plastic to elastic deformation transitions. *Nat. Electron.* **7**, 66–76 (2024).
71. L. Xue, J. T. Pham, J. Iturri, A. Del Campo, Stick–slip friction of PDMS surfaces for bioinspired adhesives. *Langmuir* **32**, 2428–2435 (2016).
72. J. A. Sandoval, S. Jadhav, H. Quan, D. D. Deheyn, M. T. Tolley, Reversible adhesion to rough surfaces both in and out of water, inspired by the clingfish suction disc. *Bioinspir. Biomim.* **14**, 066016 (2019).
73. Z. Shi, D. Tan, K. Xiao, X. Zhang, B. Zhu, Z. Lin, Q. Liu, D. Chen, Q. Zhang, L. Xue, Touch initiated on-demand adhesion on rough surfaces. *Mater. Horiz.* **11**, 3539–3547 (2024).
74. Y. Zhang, Y. Tan, J. Lao, H. Gao, J. Yu, Hydrogels for flexible electronics. *ACS Nano* **17**, 9681–9693 (2023).
75. X. Yang, Z. Wang, B. Zhang, T. Chen, C. Linghu, K. Wu, G. Wang, H. Wang, Y. Wang, Self-sensing robotic structures from architectured particle assemblies. *Adv. Intell. Syst.* **5**, 2200250 (2023).
76. X. Yang, M. Liu, B. Zhang, Z. Wang, T. Chen, Y. Zhou, Y. Chen, K. J. Hsia, Y. Wang, Hierarchical tessellation enables programmable morphing matter. *Matter* **7**, 603–619 (2024).

77. Y. Zhang, N. Zheng, Y. Cao, F. Wang, P. Wang, Y. Ma, B. Lu, G. Hou, Z. Fang, Z. Liang, M. Yue, Y. Li, Y. Chen, J. Fu, J. Wu, T. Xie, X. Feng, Climbing-inspired twining electrodes using shape memory for peripheral nerve stimulation and recording. *Sci. Adv.* **5**, eaaw1066 (2019).
78. T. Zhang, Z. Zhang, K.-S. Kim, H. Gao, An accordion model integrating self-cleaning, strong attachment and easy detachment functionalities of gecko adhesion. *J. Adhes. Sci. Technol.* **28**, 226–239 (2014).
79. M. Ciavarella, A. Papangelo, A generalized Johnson parameter for pull-off decay in the adhesion of rough surfaces. *Phys. Mesomech.* **21**, 67–75 (2018).
80. C. A. Dahlquist, R. Patrick, "Pressure-sensitive adhesives" in *Treatise on Adhesion and Adhesives* (Marcel Dekker Inc., 1969), pp. 219–260.
81. L. Gong, X. Wang, Thermal-regulated adhesion enhancement and fast switching within the viscoelastic glass transition zone of a shape memory polymer. *Langmuir* **37**, 13420–13429 (2021).
82. C. Zhao, L. Chen, Y. Ru, L. Zhang, M. Liu, Thermoresponsive ionogels with switchable adhesion in air and aqueous environments induced by LCST phase behavior. *Soft Matter* **18**, 5934–5938 (2022).
83. S. Wang, C. Zhao, S. Liu, Y. Li, Z. Xie, L. Chen, X. Yu, F. Yuan, Q. Zhang, M. Liu, L. Wen, A wearable glove with electrothermal-controlled ionogels for adhesive gripping. *Adv. Intell. Syst.* **6**, 2300127 (2023).
84. J. Huang, Y. Liu, Y. Yang, Z. Zhou, J. Mao, T. Wu, J. Liu, Q. Cai, C. Peng, Y. Xu, B. Zeng, W. Luo, G. Chen, C. Yuan, L. Dai, Electrically programmable adhesive hydrogels for climbing robots. *Sci. Robot.* **6**, eabe1858 (2021).
85. D. Wang, H. Hu, S. Li, H. Tian, W. Fan, X. Li, X. Chen, A. C. Taylor, J. Shao, Sensing-triggered stiffness-tunable smart adhesives. *Sci. Adv.* **9**, eadf4051 (2023).
86. B. Peng, Q.-A. Wang, X.-Q. Feng, Q. Li, Switchable adhesion with a high tuning ratio achieved on polymer surfaces with embedded low-melting-point alloy. *Extreme Mech. Lett.* **49**, 101488 (2021).
87. Z. Ye, G. Z. Lum, S. Song, S. Rich, M. Sitti, Phase change of gallium enables highly reversible and switchable adhesion. *Adv. Mater.* **28**, 5088–5092 (2016).
88. S. Song, D.-M. Drotlef, C. Majidi, M. Sitti, Controllable load sharing for soft adhesive interfaces on three-dimensional surfaces. *Proc. Natl. Acad. Sci. U.S.A.* **114**, E4344–E4353 (2017).
89. A. Mohammadi Nasab, A. Luo, S. Sharifi, K. T. Turner, W. Shan, Switchable adhesion via subsurface pressure modulation. *ACS Appl. Mater. Interfaces* **12**, 27717–27725 (2020).
90. W.-G. Bae, D. Kim, K.-Y. Suh, Instantly switchable adhesion of bridged fibrillar adhesive via gecko-inspired detachment mechanism and its application to a transportation system. *Nanoscale* **5**, 11876–11884 (2013).
91. B. Yoo, S. Cho, S. Seo, J. Lee, Elastomeric angled microflaps with reversible adhesion for transfer-printing semiconductor membranes onto dry surfaces. *ACS Appl. Mater. Interfaces* **6**, 19247–19253 (2014).
92. S. Seo, J. Lee, K. S. Kim, K. H. Ko, J. H. Lee, J. Lee, Anisotropic adhesion of micropillars with spatula pads. *ACS Appl. Mater. Interfaces* **6**, 1345–1350 (2014).
93. H. Tian, X. Li, J. Shao, C. Wang, Y. Wang, Y. Tian, H. Liu, Gecko-effect inspired soft gripper with high and switchable adhesion for rough surfaces. *Adv. Mater. Interfaces* **6**, 1900875 (2019).
94. Z. Shi, D. Tan, Z. Wang, K. Xiao, B. Zhu, F. Meng, Q. Liu, X. Wang, L. Xue, Switchable adhesion on curved surfaces mimicking the coordination of radial-oriented spatular tips and motion of gecko toes. *ACS Appl. Mater. Interfaces* **14**, 31448–31454 (2022).
95. V. Tinnemann, E. Arzt, R. Hensel, Switchable double-sided micropatterned adhesives for selective fixation and detachment. *J. Mech. Phys. Solids* **123**, 20–27 (2019).
96. J. Purtov, M. Frensemeier, E. Kroner, Switchable adhesion in vacuum using bio-inspired dry adhesives. *ACS Appl. Mater. Interfaces* **7**, 24127–24135 (2015).
97. H. E. Jeong, M. K. Kwak, K. Y. Suh, Stretchable, adhesion-tunable dry adhesive by surface wrinkling. *Langmuir* **26**, 2223–2226 (2010).
98. S. M. Kang, J. H. Kim, S. M. Kim, Partial wrinkle generation for switchable attachment and high adhesion hysteresis. *Int. J. Precis. Eng. Manuf.* **18**, 133–137 (2017).
99. Y. Wang, H. Tian, J. Shao, D. Sameoto, X. Li, L. Wang, H. Hu, Y. Ding, B. Lu, Switchable dry adhesion with step-like micropillars and controllable interfacial contact. *ACS Appl. Mater. Interfaces* **8**, 10029–10037 (2016).
100. X. Jin, H. Tan, Z. Wu, J. Liang, W. Miao, C. S. Lian, J. Wang, K. Liu, H. Wei, C. Feng, P. Liu, Y. Wei, Q. Li, J. Wang, L. Liu, X. Li, S. Fan, W. Duan, K. Jiang, Continuous, ultra-lightweight, and multipurpose super-aligned carbon nanotube tapes viable over a wide range of temperatures. *Nano Lett.* **19**, 6756–6764 (2019).
101. Y. Maeno, Y. Nakayama, Experimental investigation of adhesive behavior in carbon nanotube based gecko tape. *J. Adhes.* **88**, 243–252 (2012).
102. A. L. Kaiser, L. H. Acauan, A. R. Vanderhout, A. Zaman, D. L. Lidston, I. Y. Stein, B. L. Wardle, Selectively tuning the substrate adhesion strength of aligned carbon nanotube arrays via thermal postgrowth processing. *ACS Appl. Mater. Interfaces* **15**, 17029–17044 (2023).
103. Y. Cui, Y. Ju, B. Xu, P. Wang, N. Kojima, K. Ichioka, A. Hosoi, Mimicking a gecko's foot with strong adhesive strength based on a spinnable vertically aligned carbon nanotube array. *RSC Adv.* **4**, 9056–9060 (2014).
104. L. Qu, L. Dai, M. Stone, Z. Xia, Z. L. Wang, Carbon nanotube arrays with strong shear binding-on and easy normal lifting-off. *Science* **322**, 238–242 (2008).
105. G. Wan, Y. Tang, K. T. Turner, T. Zhang, W. Shan, Tunable dry adhesion of soft hollow pillars through sidewall buckling under low pressure. *Adv. Funct. Mater.* **33**, 2209905 (2023).
106. J. Seo, J. Eisenhaure, S. Kim, Micro-wedge array surface of a shape memory polymer as a reversible dry adhesive. *Extreme Mech. Lett.* **9**, 207–214 (2016).
107. S. Dai, X. Dong, Y. Jiang, J. Ge, J. Ding, N. Yuan, High adhesive force, wide temperature adaptability thermochromic ionogel smart window. *ACS Appl. Polym. Mater.* **5**, 3398–3404 (2023).
108. Y. Yan, J. Huang, X. Qiu, X. Cui, S. Xu, X. Wu, P. Yao, C. Huang, An ultra-stretchable glycerol-ionic hybrid hydrogel with reversible gelid adhesion. *J. Colloid Interface Sci.* **582**, 187–200 (2021).
109. L. Zhang, S. Wang, Z. Wang, Z. Liu, X. Xu, H. Liu, D. Wang, Z. Tian, Temperature-mediated phase separation enables strong yet reversible mechanical and adhesive hydrogels. *ACS Nano* **17**, 13948–13960 (2023).
110. M. Chen, Y. Wu, B. Chen, A. M. Tucker, A. Jagota, S. Yang, Fast, strong, and reversible adhesives with dynamic covalent bonds for potential use in wound dressing. *Proc. Natl. Acad. Sci. U.S.A.* **119**, e2203074119 (2022).
111. B. Zhang, L. Jia, J. Jiang, S. Wu, T. Xiang, S. Zhou, Biomimetic microstructured hydrogels with thermal-triggered switchable underwater adhesion and stable antiswelling property. *ACS Appl. Mater. Interfaces* **13**, 36574–36586 (2021).
112. T. S. Babra, A. Trivedi, C. N. Warriner, N. Bazin, D. Castiglione, C. Sivour, W. Hayes, B. W. Greenland, Fluoride degradable and thermally debondable polyurethane based adhesive. *Poly. Chem.* **8**, 7207–7216 (2017).
113. H. Kim, H. Mohapatra, S. T. Phillips, Rapid, On-command debonding of stimuli-responsive cross-linked adhesives by continuous, sequential quinone methide elimination reactions. *Angew. Chem. Int. Ed. Engl.* **54**, 13063–13067 (2015).
114. Y.-Z. Wang, L. Li, F.-S. Du, Z.-C. Li, A facile approach to catechol containing UV dismantlable adhesives. *Polymer* **68**, 270–278 (2015).
115. M. Kim, H. Chung, Photo-responsive bio-inspired adhesives: Facile control of adhesion strength via a photocleavable crosslinker. *Poly. Chem.* **8**, 6300–6308 (2017).
116. Y. Zhou, M. Chen, Q. Ban, Z. Zhang, S. Shuang, K. Koynov, H. J. Butt, J. Kong, S. Wu, Light-switchable polymer adhesive based on photoinduced reversible solid-to-liquid transitions. *ACS Macro Lett.* **8**, 968–972 (2019).
117. S. Saito, S. Nobusue, E. Tsuzaka, C. Yuan, C. Mori, M. Hara, T. Seki, C. Camacho, S. Irle, S. Yamaguchi, Light-melt adhesive based on dynamic carbon frameworks in a columnar liquid-crystal phase. *Nat. Commun.* **7**, 12094 (2016).
118. Y. Wang, H. Hu, J. Shao, Y. Ding, Fabrication of well-defined mushroom-shaped structures for biomimetic dry adhesive by conventional photolithography and molding. *ACS Appl. Mater. Interfaces* **6**, 2213–2218 (2014).
119. Z. Shi, B. Zhu, Z. Wang, K. Xiao, Y. Wang, L. Xue, Robust and elevated adhesion and anisotropic friction in a bioinspired bridged micropillar array. *Langmuir* **39**, 3784–3791 (2023).
120. J. Tamelier, S. Chary, K. L. Turner, Vertical anisotropic microfibers for a gecko-inspired adhesive. *Langmuir* **28**, 8746–8752 (2012).
121. Y. Wang, X. Li, H. Tian, H. Hu, Y. Tian, J. Shao, Y. Ding, Rectangle-capped and tilted micropillar array for enhanced anisotropic anti-shearing in biomimetic adhesion. *J. R. Soc. Interface* **12**, 20150090 (2015).
122. H. E. Jeong, J.-K. Lee, H. N. Kim, S. H. Moon, K. Y. Suh, A nontransferring dry adhesive with hierarchical polymer nanohairs. *Proc. Natl. Acad. Sci. U.S.A.* **106**, 5639–5644 (2009).
123. K. Jin, J. C. Cremaldi, J. S. Erickson, Y. Tian, J. N. Israelachvili, N. S. Pesika, Biomimetic bidirectional switchable adhesive inspired by the gecko. *Adv. Funct. Mater.* **24**, 574–579 (2014).
124. H. S. Im, K. Y. Kwon, J. U. Kim, K. S. Kim, H. Yi, P. J. Yoo, C. Pang, H. E. Jeong, T. I. Kim, Highly durable and unidirectionally stooped polymeric nanohairs for gecko-like dry adhesive. *Nanotechnology* **26**, 415301 (2015).
125. T. I. Kim, H. E. Jeong, K. Y. Suh, H. H. Lee, Stooped nanohairs: Geometry-controllable, unidirectional, reversible, and robust gecko-like dry adhesive. *Adv. Mater.* **21**, 2276–2281 (2009).
126. H. Yoon, H. E. Jeong, T. I. Kim, T. J. Kang, D. Tahk, K. Char, K. Y. Suh, Adhesion hysteresis of Janus nanopillars fabricated by nanomolding and oblique metal deposition. *Nano Today* **4**, 385–392 (2009).
127. Z. Wang, P. Gu, X. Wu, Gecko-inspired bidirectional double-sided adhesives. *Soft Matter* **10**, 3301–3310 (2014).
128. K. Jin, Y. Tian, J. S. Erickson, J. Puthoff, K. Autumn, N. S. Pesika, Design and fabrication of gecko-inspired adhesives. *Langmuir* **28**, 5737–5742 (2012).
129. Z. Wang, Slanted functional gradient micropillars for optimal bioinspired dry adhesion. *ACS Nano* **12**, 1273–1284 (2018).
130. L. Ge, S. Sethi, L. Ci, P. M. Ajayan, A. Dhinojwala, Carbon nanotube-based synthetic gecko tapes. *Proc. Natl. Acad. Sci. U.S.A.* **104**, 10792–10795 (2007).

131. Z. Rong, Y. Zhou, B. Chen, J. Robertson, W. Federle, S. Hofmann, U. Steiner, P. Goldberg-Oppenheimer, Bio-inspired hierarchical polymer fiber–carbon nanotube adhesives. *Adv. Mater.* **26**, 1456–1461 (2014).
132. T. Zhang, H. Yuk, S. Lin, G. A. Parada, X. Zhao, Tough and tunable adhesion of hydrogels: Experiments and models. *Acta Mech. Sin.* **33**, 543–554 (2017).
133. R. W. Ogden, D. G. Roxburgh, A pseudo–elastic model for the Mullins effect in filled rubber. *Proc. R. Soc. London Ser. A* **455**, 2861–2877 (1999).
134. E. Sancaktar, Fracture aspects of adhesive joints: Material, fatigue, interphase, and stress concentration considerations. *J. Adhes. Sci. Technol.* **9**, 119–147 (1995).
135. P. P. Camanho, C. G. Davila, M. De Moura, Numerical simulation of mixed-mode progressive delamination in composite materials. *J. Compos. Mater.* **37**, 1415–1438 (2003).

Acknowledgments: We express our appreciation to X. Chen (Nanyang Technological University) and P. S. Lee (Nanyang Technological University) for support in experiments and our lab colleagues, Y. Tang (Nanyang Technological University) and A. Zhou (Nanyang Technological University), for assistance during the experiments. We also thank K. Liu (Peking University) for input on the data visualization. **Funding:** K.J.H., H.G., and C.L. acknowledge the support by the Ministry of Education (MOE) of Singapore under Academic Research Fund Tier 2 (MOE-T2EP50122-0001). C.L. also acknowledges a Graduate Research Scholarship supported by the MOE of Singapore (G2001924H). Y.W. acknowledges the NAP award (020482) from Nanyang Technological University. **Author contributions:** Conceptualization: C.L., Y.F., H.G., and K.J.H. Methodology: C.L., Yangchengyi Liu, X.Y., Z.C., Y.Z., Y.-J.S., X.W., Y.W., H.G., and K.J.H. Software: C.L., X.Y., Z.C., J.F., and Z.Z. Validation: C.L., Yangchengyi Liu, X.Y., Y.L., Z.Z., Y.-J.S., J.L., H.J., Y.W., and H.G. Formal analysis: C.L., Yangchengyi Liu, J.F., Y.-J.S., H.J., Yuhang Li, K.J.H. Investigation: C.L., Yangchengyi Liu, J.F., Yan Li, Y.-J.S., J.L., H.J., J.S., Yuhang Li, and K.J.H. Resources: C.L., Y.-J.S., J.F., Y.F., Y.W., H.G., and K.J.H. Data curation: C.L., Yangchengyi Liu, Y.-J.S., H.J., J.F., and K.J.H. Writing—original draft: C.L., Yangchengyi Liu, X.Y., Z.C., X.W., Y.W., H.G., and K.J.H. Writing—review and editing: C.L., Yangchengyi Liu, X.Y., Z.C., Y.-J.S., H.J., Y.F., X.W., Y.W., H.G., and K.J.H. Visualization: C.L., Yangchengyi Liu, X.Y., Z.C., J.F., Y.Z., Y.F., X.W., Y.W., and K.J.H. Supervision: C.L., Y.F., X.W., Y.W., H.G., and K.J.H. Project administration: C.L., X.W., Y.W., H.G., and K.J.H. Funding acquisition: Y.W., H.G., and K.J.H. **Competing interests:** The authors declare that they have no competing interests. **Data and materials availability:** All data needed to evaluate the conclusions in the paper are present in the paper and/or the Supplementary Materials.

Submitted 27 September 2024
Accepted 17 December 2024
Published 17 January 2025
10.1126/sciadv.adt4765